Monatshefte für Chemie - Chemical Monthly (2025) 156:1089–1099
https://doi.org/10.1007/s00706-025-03367-9

ORIGINAL PAPER

Waste carbon and carbon nanotube composite paste electrode for ferulic acid detection

K. P. Moulya[1] · J. G. Manjunatha[1] · V. Nandakumar[2] · D. K. Ravishankar[3] · Ashok S. Alur[4] · Nagaraja Sreeharsha[5] · T. C. Canevari[6]

Received: 17 July 2025 / Accepted: 1 August 2025 / Published online: 13 August 2025

Abstract

Waste carbon and carbon nanotubes were combined to create a polymer-modified composite paste electrode. The improved electrode's electrochemical analysis and effectiveness for the electrocatalytic oxidation of ferulic acid were reported. The sensor was used to examine the electrocatalytic oxidation of ferulic acid utilizing cyclic voltammetry and differential pulse voltammetry as diagnostic methods. It has been discovered that the modified surface of the electrode oxidizes ferulic acid with a higher current response than that of an unmodified electrode. For ferulic acid, DPV shows a detection limit of 0.513 µM and a linear dynamic range of 0.2 µM to 4.0 µM. A simultaneous study also conducted with vanillin, the produced sensor showed exceptional sensitivity and selectivity. Finally, the ferulic acid in the genuine sample was determined using the modified electrode.

Graphical Abstract

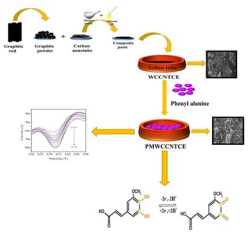

Keywords Ferulic acid · Vanillin · Waste carbon · Carbon nanotube · Sensing · Electrochemical analysis · Polymer modification

✉ J. G. Manjunatha
manju1853@gmail.com

1 Department of Chemistry, FMKMC College, Constituent College of Mangalore University, Madikeri, Karnataka, India

2 Department of Physics, Maharani's Science College for Women (Autonomous), Mysuru, Karnataka 570005, India

3 Department of Chemistry, Maharanis Science College for Women (Autonomous), University of Mysore, Mysuru, Karnataka, India

4 Kodagu University, Thorenur, Karnataka, India

5 Department of Pharmaceutical Sciences, College of Clinical Pharmacy, King Faisal University, 31982 Al-Ahsa, Saudi Arabia

6 Institute of Chemistry, State University of Campinas, PO Box 6154, 13,084–971, Campinas, SP, Brazil

Introduction

The identification of clinically significant compounds and their metabolites is essential for both developing clinical diagnostics and comprehending their biological and physiological roles [1]. Ferulic acid (FA) is a phenolic molecule that has strong antibacterial properties. It has a benzene ring, methoxy and hydroxyl groups, and a double bond on the side. Numerical physiological functions are exhibited by FA, such as anti-inflammatory [2], anti-aging [3], antioxidant [4], anti-ultraviolet radiation [5], antithrombotic properties [6], hepatoprotective effects [7], neuroprotective [8], and vasculoprotective [9]. FA has been extensively used in the fields of nutritious foods, cosmetics, and medicine

[10]. As a result, a reliable and simple technique should be developed to detect FA. High-performance liquid chromatography [11–14], UV–Vis spectrophotometry [15], mass spectrometry [16], fluorescence [17], thin-layer chromatography [18], and high-performance capillary electrophoresis [19] are the most commonly used methods for the detection of FA. However, because these techniques require pretreatment processes, expensive equipment, and are often time-consuming, they may not be suitable for the clinical screening of FA. Vanillin (VN) is the flavoring agent widely used in food industries; it also possesses antioxidant properties. Hence, it was chosen for the simultaneous analysis with FA. A variety of techniques are available for the analytical assessment of these compounds, applicable in both in vitro and in vivo conditions. Electrochemical methods in clinical analysis provide the potential to achieve selective, rapid, in situ, sensitive, and low-cost detection of biomolecules that are crucial for clinical analysis and for monitoring the diseases treatment [20–24]. Therefore, the electrochemical technique is a feasible method that can be utilized for the detection of FA. Previous studies examined the electrochemical behavior of FA and used different working electrodes to quantitatively determine FA, such as glassy carbon electrode (GCE) [25], carbon nanofiber-based screen-printed sensor [26], polypyrrole-multiwalled carbon nanotubes [27], and carbon paste electrode [28]. However, these works have many drawbacks, such as availability, affordability, long electrode preparation procedures, etc.; hence, a sensor needs to be developed to overcome these drawbacks. The performance of the developed sensor depends on the properties of a modifier that affects the sensitivity and selectivity of these sensors towards the detection of FA.

Three electrodes—working electrodes, indicating electrodes, and supporting electrodes—are the foundation of the electrometric detection method known as voltammetry. In the monitoring system, each electrode plays a distinct function. Redox reactions take place through the working electrode. Information on the potential value and current will be revealed by the redox reaction that takes place. The potential value produced by the working electrode is stabilized in part by the reference electrode. The auxiliary electrode functions as a pair of working electrodes in the meanwhile; if the working electrode undergoes an oxidation reaction, the auxiliary electrode undergoes a reduction reaction, and vice versa [29, 30]. Researchers throughout the world are now studying functioning electrodes in broad applications. Much attention has been paid to the design of the detecting system that uses novel electrodes. Carbon electrodes and their derivatives, including glassy carbon [31], graphene [32, 33], graphene oxide [34], carbon quantum dots [35], carbon nanotubes [36, 37], carbon paste [38, 39], and other carbon materials [40, 41], are the most often employed working electrodes. Furthermore, a number of functional electrodes have been documented, including silver [42], platinum [43], gold [44], bimetallic platinum-gold [45], and alloys [46, 47]. Researchers are concentrating not just on creating new electrodes but also on altering existing electrodes to improve sensitivity or selectivity.

In this study, we adjusted and investigated the potential of phenylalanine (PA) as a clever modifier for carbon derived from waste battery and carbon nanotube electrodes in the detection of FA, in contrast to the modifiers that have been reported by several studies. The goal of the electropolymerized BWCCNTCE in the current work is to produce a polymer-modified composite paste electrode surface for FA resolution. This method was also used to quantify FA and VN simultaneously. Determining FA in a real sample further examined the analytical use of the fabricated electrode.

Results and discussions

Preparation of PMWCCNTCE

Phenylalanine (PA) was electro-polymerized on the bare waste carbon and carbon nanotube composite electrode (BWCCNTCE) surface using the cyclic voltammetry (CV) process to create the polymer-modified waste carbon and carbon nanotube composite paste electrode (PMWCCNTCE). In an electrolytic cell with phosphate buffer solution (PBS) at pH 7.0 and 1.0 mM PA, the BWCCNTCE surface was scanned ten times at 0.1 V/s of scan rate throughout the potential window of −1.25 to 1.75 V. The formation of the poly(PA) layer on the BWCCNTCE surface is shown by the current value gradually increasing as the number of polymerization cycles increases throughout this electropolymerization process. Figure 1a displays the CVs generated during this procedure. The BWCCNTCE surface develops a conductive layer of poly(PA) that improves the electrode's sensing capabilities for target analyte analysis. To get rid of the unreacted monomers, the electrode's exterior was cleaned with double-distilled water once this procedure was finished. Figure 1b displays the current response for 1.0 mM FA at PMWCCNTCE for different numbers of polymer cycles of PA. The maximum response was at 10 cycles; hence, it was chosen for further analysis of FA.

Electrode characterization by SEM

The BWCCNTCE and PMWCCNTCE SEM images are displayed in Fig. 2. The two electrodes' surface configurations differ greatly from one another. It was discovered that a micrometer-sized, uneven paste constituted the surface of BWCCNTCE (Fig. 2a). They entangled to create a network structure once the polymer film was uniformly dispersed across the electrode surface (Fig. 2b). It can speed up the

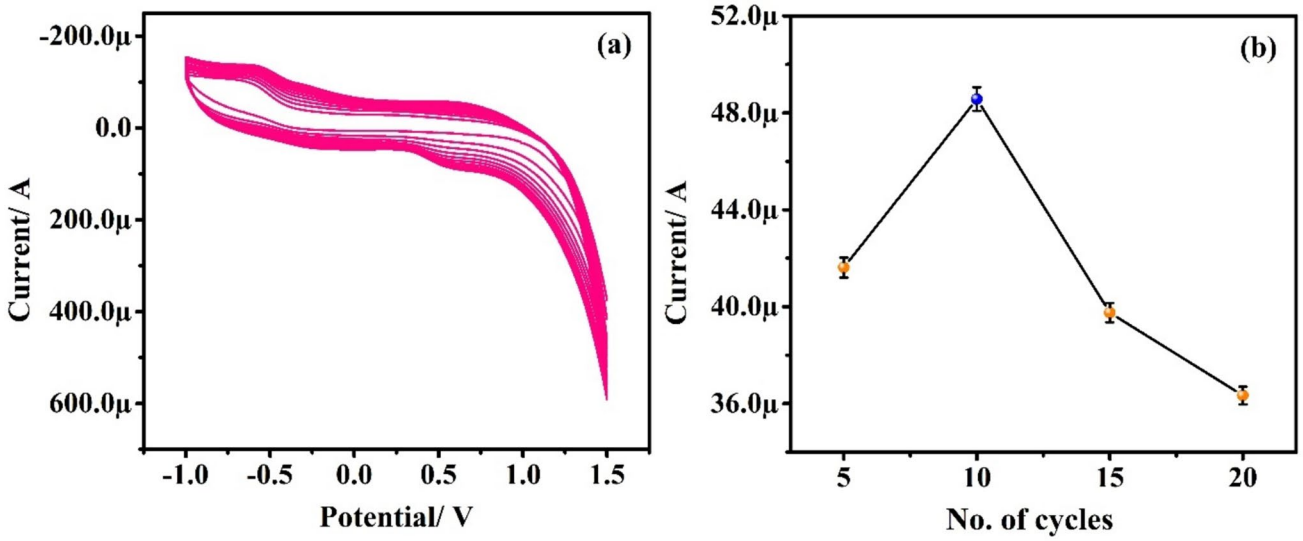

Fig. 1 **a** CVs for 10 cycles of 1.0 mM PA on BWCCNTCE at the scan rate of 0.1 V/s in 0.2 M PBS of pH 7.0; **b** plot of current versus number of cycles for 1.0 mM FA

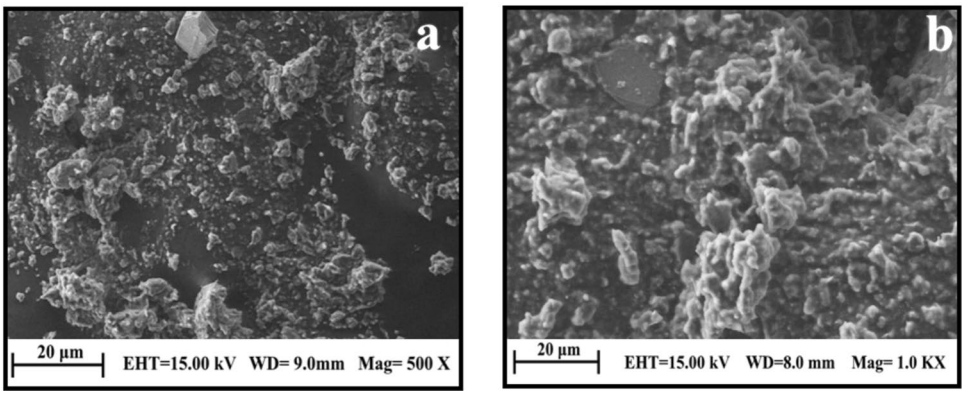

Fig. 2 SEM descriptions of **a** BWCCNTCE and **b** PMWCCNTCE

pace of electron transport and significantly expand the electrode surface's active surface area.

Study of active surface area

The surface area of the electrodes can be easily and effectively analyzed using CV technique. Figure 3 displays the CVs of two different sensors, BWCCNTCE (curve a) and PMWCCNTCE (curve b) for 1.0 mM $K_4[Fe(CN)_6]$ in 0.1 M KCl solution. With cathodic–anodic peak potential (E_{pa}), peak potential (E_{pc}), and peak-to-peak separation (ΔE_p) of 0.011 V, 0.393 V, and 381 mV, respectively, the redox process of $K_4[Fe(CN)_6]$ is quasi-reversible at BWCCNTCE (curve a). In contrast to BWCCNTCE, the peak response of $K_4[Fe(CN)_6]$ during PMWCCNTCE sharply rose, while ΔE_p decreased to 70 mV (curve b). The findings demonstrate that PMWCCNTCE can increase the rate of electron transport.

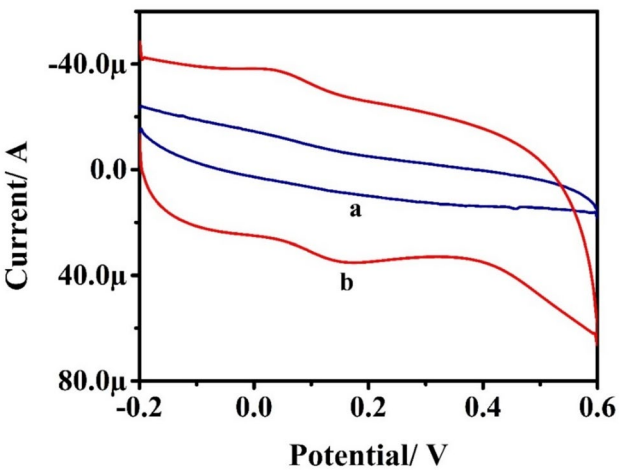

Fig. 3 CVs for 0.1 mM $K_4[Fe(CN)_6]$ dispersed in 0.1 M KCl at the surface of BWCCNTCE (curve a) and PMWCCNTCE (curve b)

Composite paste and polymer film had a synergistic impact on sensor performance, as seen by the large increase in redox peak currents that occurred when polymer was used to alter the surface. This rise was primarily caused by an increase in effective surface area and conductivity. As per Randles–Sevcik formula, Eq. (1) [48]:

$$I_{pa} = 2.69 \times 10^5 n_2^3 A D_2^1 C v_2^1 \quad (1)$$

I_{pa} stands for peak current (A), A for effective area (cm^2), n for number of electrons transferred, ν for scan rate (V/s), D for $K_4[Fe(CN)_6]$ diffusion coefficient (7.6×10^{-6} cm^2 s^{-1}), and C for bulk concentration of $K_4[Fe(CN)_6]$. The calculation above indicates that PMWCCNTCE has a greater electroactive surface area of 0.056 cm^2 than BWCCNTCE, measuring 0.026 cm^2. The findings demonstrate that polymer film and composite paste may greatly expand the electrode's effective area and quicken the electron transmission.

Electrochemical performance of the developed sensors

The Nyquist diagrams of electrochemical impedance spectroscopy (EIS) measurements are displayed in Fig. 4. By fitting the recorded EIS database to the standard Randles equivalent circuit model, which includes the charge transfer resistance (R_{ct}), the electrochemical parameters of the electrodes and electrode–electrolyte interface are determined. A Nyquist diagram contains two parts: (1) a linear part at low frequency that describes the diffusion process, and (2) a semicircle at high frequency, where the diameter relates to R_{ct}.

The BWCCNTCE (curve a) and PMWCCNTCE (curve b) electrodes had R_{ct} values of 281.5 Ω and 226.9 Ω, respectively. This suggests that the PMWCCNTCE has a higher electron transfer rate than the BWCCNTCE electrode. It proves that FA's impact on the PMWCCNTCE electrode's sensitivity results from the modifier's conductive effect. It is notable that the Nyquist diagrams have a linear component part, which suggests that the electrochemical reactions at the electrode are diffusion-limited.

Oxidation behavior of FA at BWCCNTCE and PMWCCNTCE

The voltammetric response of FA at the PMWCCNTCE and BWCCNTCE has been compared to analyze the sensitivity of the developed sensors. At a sweep rate of 0.1 V/s, Fig. 5 shows the CVs for 1.0 mM FA at polymer modified CNT (PMCNTCE) (curve b), polymer modified waste carbon electrode (PMWCE) (curve c), BWCCNTCE (curve d), PMWCCNTCE (curve e), and blank determination (without FA, curve a) in the supporting electrolyte (pH 4.5 of 0.2 M PBS). While the increased voltammetric signal of FA (I_{pa} = 49.29 µA, E_{pa} = 0.401 V) at the modified electrode indicates the detecting capabilities of the modified sensor over BWCCNTCE, the analytical signal of the FA on the BWCCNTCE was negligible (I_{pa} = 35.53 µA, E_{pa} = 0.403 V). In order to detect FA, the PMWCCNTCE was used as a sensing material.

Effect of pH

Since the redox process will be significantly impacted by the protonation mechanism of organic molecules, CV evaluated pH optimization. In solutions with values of pH ranging from 3.5 to 6.0, the effect of the supporting

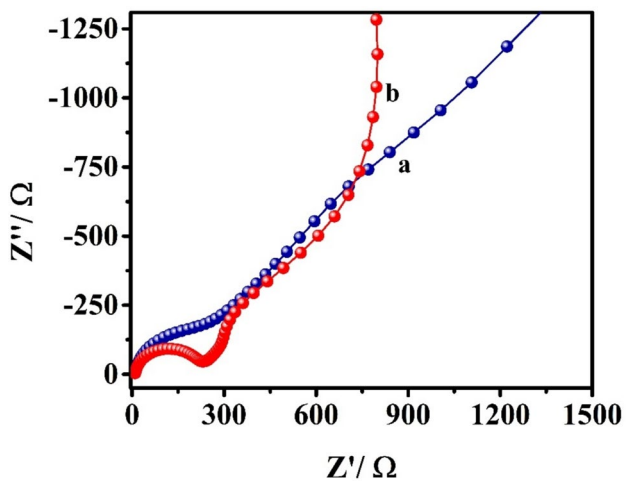

Fig. 4 Nyquist plot for 0.1 mM $K_4[Fe(CN)_6]$ contained in 0.1 M KCl at BWCCNTCE (curve a) and PMWCCNTCE (curve b)

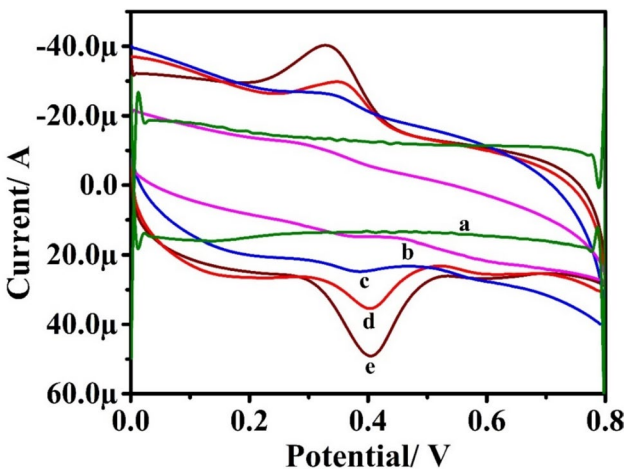

Fig. 5 CVs for blank (without FA, curve a) at PMWCCNTCE and 1.0 mM FA in pH 4.5 of 0.2 M PBS at PMCNTCE (curve b), PMWCE (curve c), BWCCNTCE (curve d), and PMWCCNTCE (curve e) at 0.1 V/s scan rate

electrolyte on the electro-oxidation of FA was scrutinized. Due to insufficient protons, FA showed a modest electrochemical response at higher pH values, with the largest peak sensitivity occurring at pH 4.5 (Fig. 6a). The plot of E_{pa} vs. pH (Fig. 6c) showed a linear relation, with the oxidative potentials steadily declining towards the less positive side as pH increased. This linear shift in peak potential was most likely caused by the deprotonation process that occurs during the analyte's oxidation. With $R^2 = 0.9897$, the linear regression equation is written as E_{pa} (V) = 0.595–0.043 pH. The slope value provides insight into the role of protons and electrons. Scheme 1 illustrates the likely electrochemical process. As can be seen from the I_{pa} vs. pH plot (Fig. 6b), the peak current rises from pH 3.5 to pH 4.5 before declining. Since physiological pH produced the most advantageous electro-oxidation of FA, pH 4.5 was deemed ideal for more research.

Scheme 1

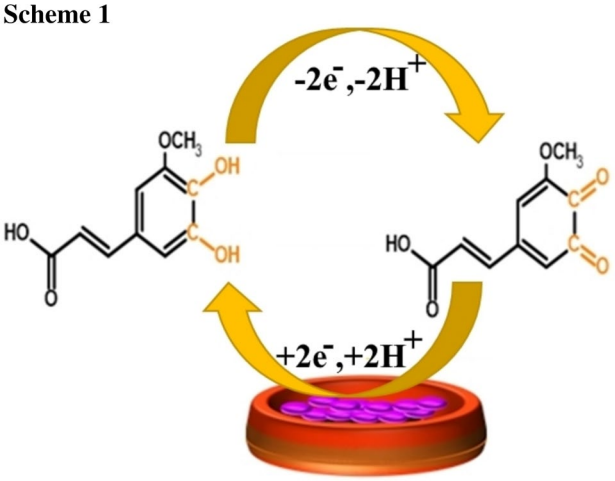

Scheme 1 Probable mechanism of electrochemical oxidation of FA

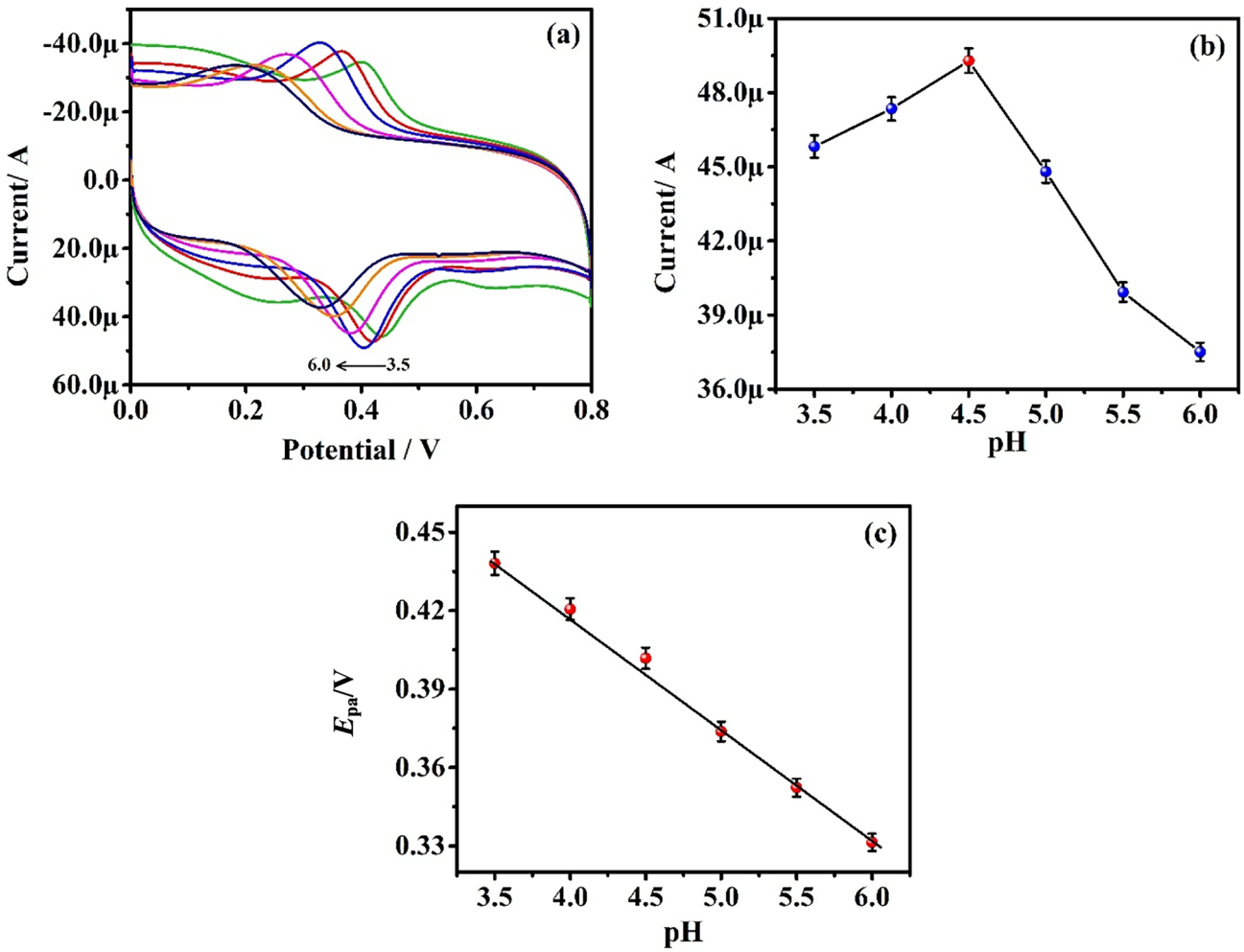

Fig. 6 **a** CVs of 1.0 mM FA in pH range of 3.5 to 6.0 of 0.2 M PBS at the scan rate of 0.1 V/s at PMWCCNTCE; **b** plot of I_{pa} vs. pH; **c** plot of E_{pa} vs. pH

Scan rate study

Analyzing the scan rate result allows one to infer the electrochemical interaction of the analyte at the sensor surface. In this investigation, the CVs for 1.0 mM FA in a 0.2 M supporting electrolyte (pH 4.5) were recorded on the suggested sensor at different scan speeds ranging from 0.025 to 0.400 V/s (Fig. 7a). The characteristic of the quasi-reversible reaction is that as the scan rate increased, the E_{pa} changed towards the more positive side, as the CVs suggest. Figure 7b displayed the scan rate versus I_{pa} plot, demonstrating linearity, and the related linear regression equation is as follows:

$$I_{pa}(\mu A) = 1.022 \times 10^{-5} + 4.142 \times 10^{-4} v(V/s)\left(R^2 = 0.997\right) \quad (2)$$

The aforementioned finding indicates that the FA oxidation reaction is an adsorption-controlled process. To verify this, a log I_{pa} vs. log ν (Fig. 7c) graph was created, and the linear fit equation is shown as follows:

$$\log I_{pa}(\mu A) = -3.417 + 0.864 \log v(V/s)\left(R^2 = 0.999\right) \quad (3)$$

Equation (3) yielded a gradient value of 0.864, which was quite near to the predicted value of 1.0, confirming that adsorption regulated the electrode response. The aforementioned findings demonstrate the interdependence between scan rate, I_{pa}, and E_{pa}. The number of electrons involved in the reaction of FA was found to be 1.8 ≈ 2.0, which was obtained using Laviron's equation as follows [49]:

$$E_{pa}(\mathrm{V}) = 0.481 + 0.065 \log v(\mathrm{V/s})\left(\mathrm{R}^2 = 0.941\right) \quad (4)$$

$$E_{pa} = E^0 + \left(\frac{RT}{(1-\alpha)nF}\right)\ln v \quad (5)$$

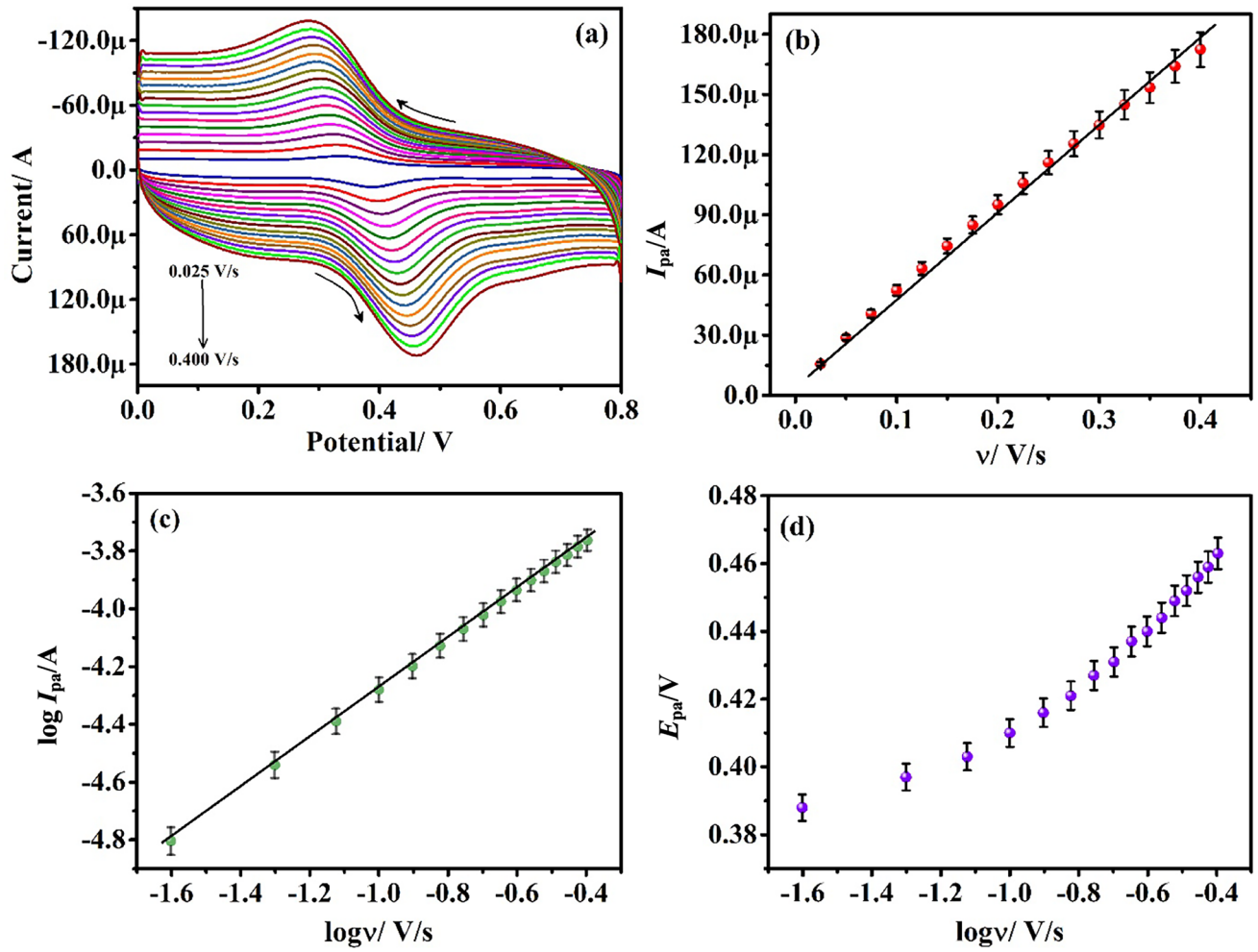

Fig. 7 **a** CVs for 1.0 mM FA in pH 4.5 at PMCCNTCE for scan rate range of 0.025–0.400 V/s; **b** plot of I_{pa} vs. ν; **c** graph of log I_{pa} vs. log ν; **d** graph of E_{pa} vs. log ν

where E_{pa} is the slope value obtained from the graph of Fig. 7d and the linear regression equation corresponding to this is depicted in Eq. (4), E^0 indicates the standard electrode potential, R represents the universal gas constant, T represents the temperature, α designates the charge transfer coefficient, F signifies the Faraday's constant, n indicates the number of electrons, and ν is the scan rate. The possible electrochemical reaction of FA involving two electrons and two protons is depicted in Scheme 1.

Calibration plot and limit of detection

Differential pulse voltammetry (DPV) mode was used in order to provide a sensitive voltammetric surface for the measurement of FA. The regression equation derived from the calibration plot was used to determine the detection limit, which under ideal conditions ranged from 0.2 to 4.0 µM FA. Figure 8 displays the calibration graph and DPVs. The adsorption of the oxidation product on the sensor surface causes the calibration plot's linearity to decrease at concentrations more than 5.0 µM. The voltammograms clearly show a modest shift in potential towards positivity, indicating that the product generated undergoes adsorption at the PMWCCNTCE surface. I_{pa} (µA) = 3.532 + 6.738 × 10^{-5} [FA] (M) (R^2 = 0.9643) was the linear regression equation derived from the calibration graph. The statistical terms limit of detection (LOD = 3 × Standard deviation of blank / slope of the linear curve) and limit of quantification (LOQ = 10 × Standard deviation of blank / slope of the linear curve) [50] were determined to be 0.513 µM and 1.71 µM, respectively. Table 1 compares the suggested electrode's detection limit to the previously published electrodes.

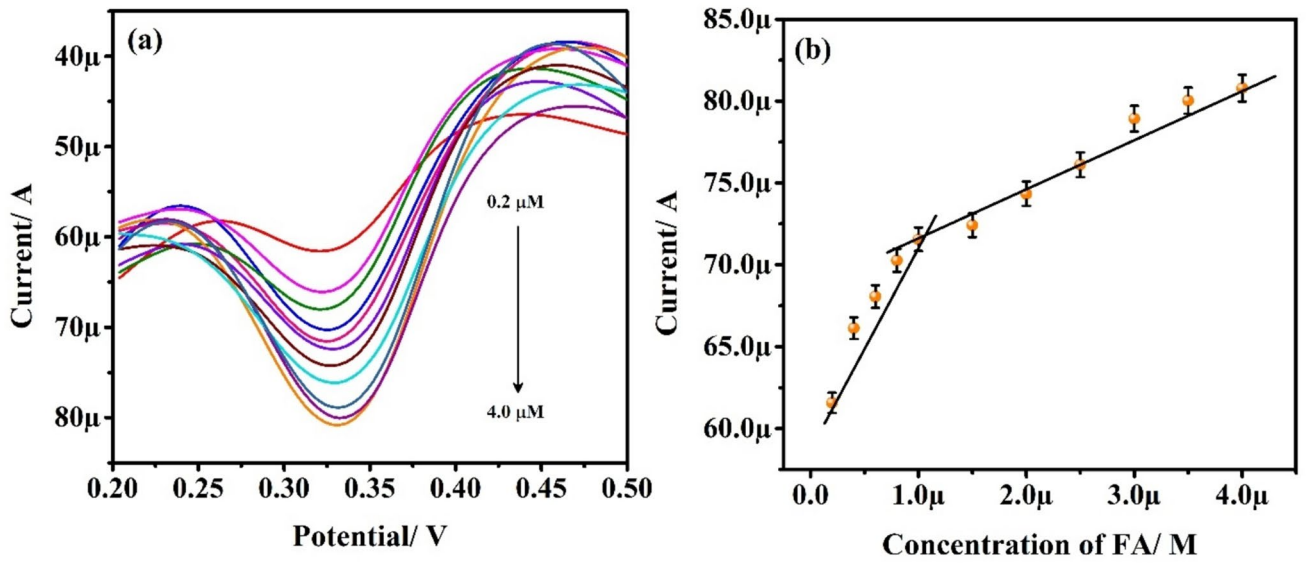

Fig. 8 **a** DPVs for 1.0 mM FA in the range of 0.2 µM to 4.0 µM in 4.5 pH of 0.2 M PBS at PMWCCNTCE; **b** calibration graph of current vs. concentration of FA

Table 1 Comparison of PMWCCNTCE with the published works

Electrode	Technique	Linear range/µM	LOD/µM	References
g-C_3N_4/CS/GCE	DPV	5.0–30.0	4.96	[51]
PPy-MWCNTs/GCE	SWV	3.32–25.9	1.17	[52]
MWCNTs-GCE	DPV	2.0–10.0	1.00	[53]
CNF/SPE	CV	10.0–1000	0.23	[26]
$MnFe_2O_4$/MIM-PF_6/CPE	DPV	0.3–250	0.1	[54]
DDAB/nafion/CPE	CV	2.0–1200	0.39	[55]
Nano-biochar/GCE	DPV	0.5–50.0	0.2	[56]
CNF/SPE	CV	10–1000	0.778	[26]
PMWCCNTCE	DPV	0.2–4.0	0.513	Present work

Stability, repeatability, and reproducibility

The sensing performance is expected to be dependent on criteria such as stability, repeatability, and reproducibility. Four trials of 1.0 mM FA in pH 4.5 of 0.2 M PBS were conducted to examine repeatability in an ideal condition at PMWCCNTCE. The measured RSD value was 1.53%. Reproducibility was demonstrated by separately testing four electrodes with 1.0 mM FA at pH 4.5. The expected RSD came to 2.02%. After 1 week, the storage stability of PMWCCNTCE for the FA determination remained at 92.5%. For the electrochemical oxidation of FA, the improved electrode therefore exhibits satisfactory stability. A bar graph representation of the results obtained is depicted in Fig. 9.

Simultaneous resolution of FA with VN

It is crucial to identify FA and VN at the same time because they are commonly found together in most confections. The CV, DPV, and linear scanning voltammetry (LSV) approach was utilized to detect FA and VN concurrently at BWCCNTCE and PMWCCNTCE in PBS of pH 4.5. Figure 9 displays the curves for 1.0 mM FA and 1.0 mM VN at BWCCNTCE (curve a) and PMWCCNTCE (curve b) for different techniques like CV (Fig. 9a), DPV (Fig. 9b), and LSV (Fig. 9c). The well-separated concavity for FA in the presence of VN suggests that simultaneous detection at the modified electrode is not impossible. However, these molecules cannot be detected at BWCCNTCE since the peaks showed negligible response at the unaltered electrode (Fig. 10).

Interference study

One of a novel sensor's most important characteristics is its selectivity. The influence of a range of substances as compounds possibly interfering with the detection of FA was examined under the optimal condition with 1.0 mM FA at

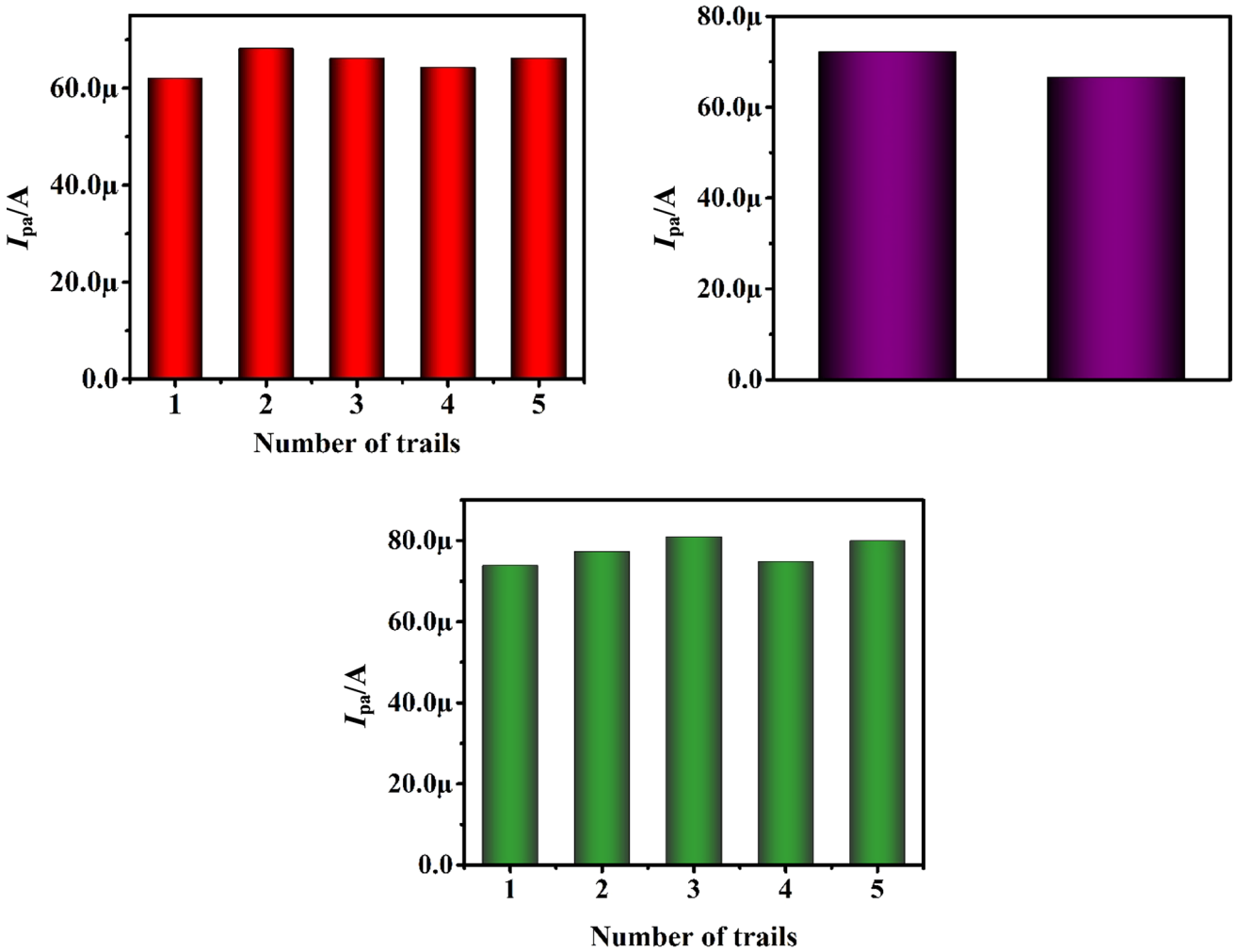

Fig. 9 Graphical representation of reproducibility, repeatability, and stability

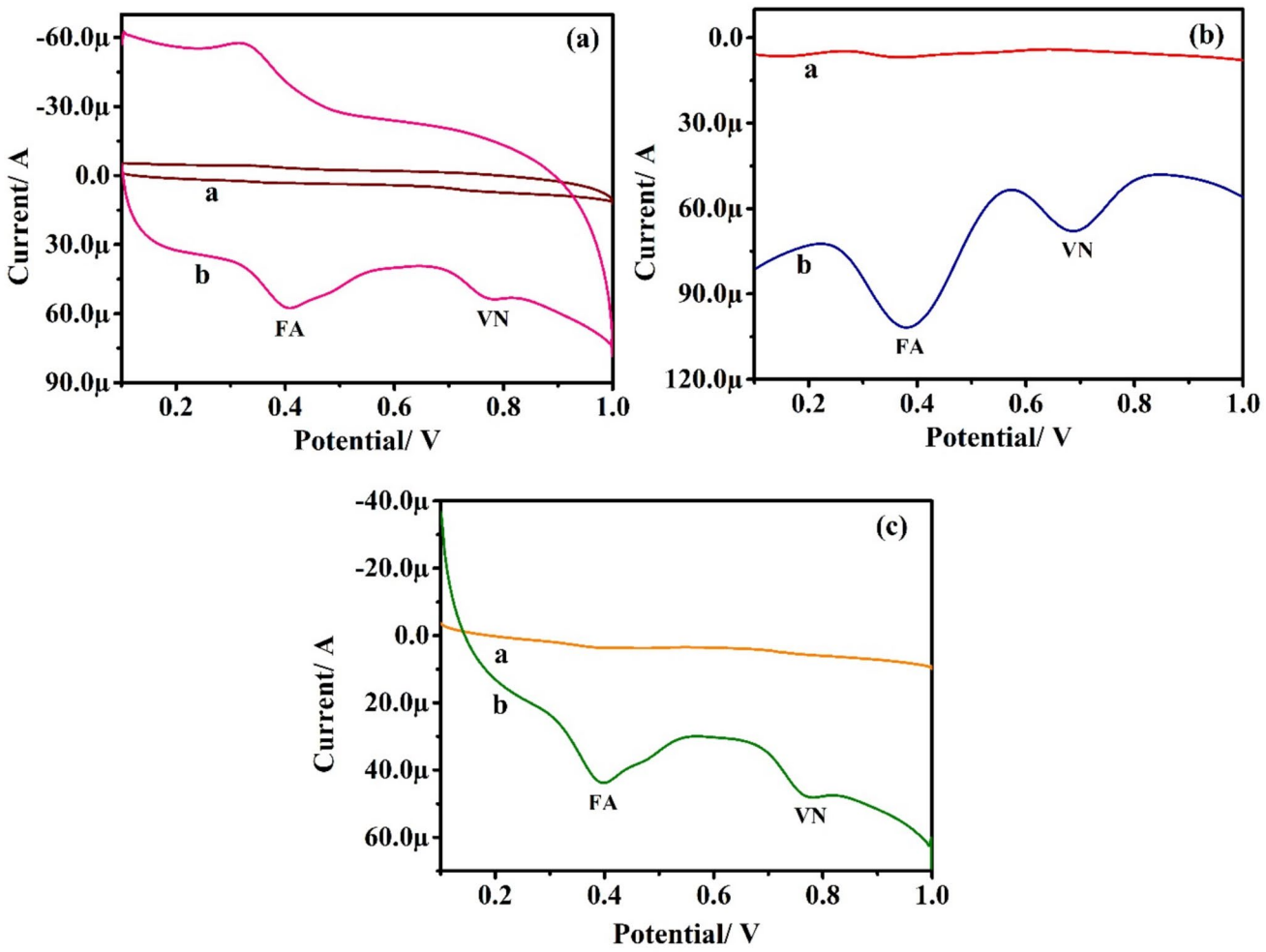

Fig. 10 **a** CVs for 1.0 mM FA and 1.0 mM VN in pH 4.5 of 0.2 M PBS at BWCCNTCE (curve a) and PMCCNTCE (curve b); **b** DPVs for 1.0 mM FA and 1.0 mM VN in pH 4.5 of 0.2 M PBS at BWCCNTCE (curve a) and PMCCNTCE (curve b); **c** LSVs for 1.0 mM FA and 1.0 mM VN in pH 4.5 of 0.2 M PBS at BWCCNTCE (curve a) and PMCCNTCE (curve b)

pH 4.5. Under ideal circumstances, the interference test was conducted with cations, including Co^{2+}, Ca^{2+}, K^{+}, Mg^{2+}, Zn^{2+}, Na^{+}, and organic compounds like amaranth (AM), caffeic acid (CA), fast green (FG), eugenol (EU), curcumin (CU), tartrazine (TZ), rutin (RU), and riboflavin (RF). The oxidation potential of FA was found to be unaffected by cations and other organic compounds. The outcome demonstrates that the suggested electrode for the electroanalysis of FA has a good capacity to tolerate interference and the tolerance limit was less than ± 5; the results are depicted in Fig. 11.

Real sample analysis and test for recovery

The commercially available jowar powder was bought from the local market and subjected to a CV technique to assess the developed electrode's viability. The analysis was conducted in accordance with the FA content of that particular

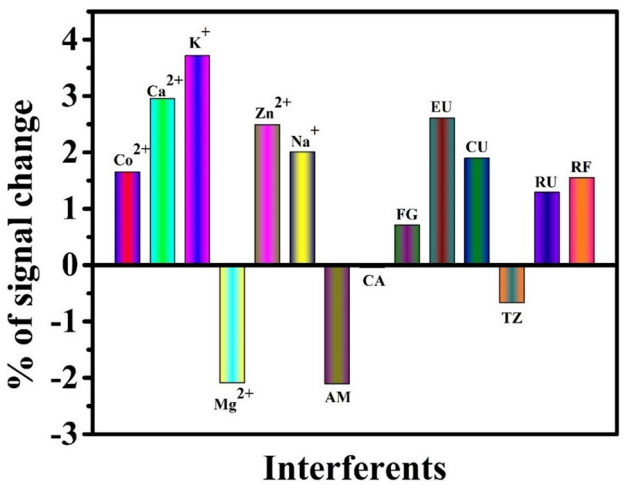

Fig. 11 Plot of % of signal change vs. interferents

Table 2 Real sample analysis of FA in jowar powder

Sample	Added/μM	Found/μM	Recovery/%
Jowar powder	2.4	2.37	99.12
	2.6	2.60	100.2
	2.8	2.77	98.97
	3.0	3.03	101.13

sample. By the utilization of obtained data, we computed the recovery of the sample and are gathered in Table 2. The observed recovery values (98.97–101.13%) show that the recently constructed electrode may be effectively employed for the detection of FA in actual samples.

Conclusion

FA was determined by CV, DPV, and LSV using a modified electrode (based on waste carbon and carbon nanotubes) with polymerization by PA. This electrode was created for the voltammetric detection of FA. By using SEM, CV, and EIS techniques, the surface characterization of the developed electrode was clarified, and it was discovered that its repeatability, reproducibility, and applicability were successful. Ultimately, the DPV technique and PMWCCNTCE were effectively used to determine the LOD in the linear range of 0.2–4.0 μM and was found to be 0.513 μM. The developed PMWCCNTCE showed a recovery rate of 98.97–101.13% in jowar powder sample for FA. Due to affordability and environmental approach, the developed sensor can be considered for the analysis of FA in real samples.

Experimental

Every reagent utilized in this investigation was purchased commercially and was of analytical reagent quality. FA (98% purity) was procured from Tokyo Chemical Industry, Japan. VN (99% purity) was purchased from Medilise Chemicals, India. For the electrode production, MWCNTs with a superficial diameter of 110–170 nm and a length of 5–9 μm were purchased from Sisco Research Laboratory Pvt. Ltd, India. HiMedia Laboratories in India supplied the sodium salts of monobasic phosphate (NaH_2PO_4) (99.5% purity) and dibasic phosphate (Na_2HPO_4) (99% purity). We obtained potassium chloride (KCl) (99.5% purity) from Nice Chemicals, India. By properly dissolving the estimated amounts of the corresponding compounds in deionized water, FA and VN solutions with a concentration of 1.0 mM were created. By carefully combining the required concentrations of 0.2 M Na_2HPO_4 and NaH_2PO_4 solutions, phosphate buffer solution (PBS) with the appropriate pH was produced.

For all voltammetric procedures, an electrochemical analyzer of model CHI-6038E (CH Instruments, USA) was employed. A three-electrode system, including a reference electrode of $Hg/HgCl_2$, an auxiliary electrode of Pt wire, a working electrode composed of waste carbon, and a carbon nanotube-based composite sensor, was incorporated. A computer system in the electrochemical analyzer saved the data that was collected. The VITSIL-VBSD/VBDD setup was used to acquire distilled water required for the analysis. Room temperature, or 25 ± 1 °C, was used for all measurements.

Extraction of electrode material

To discharge the batteries, they were submerged in a 5% NaCl solution for 24 h. The graphite rod was manually disassembled and separated, and it was crushed into a fine residue. The resulting powder was then heated in a furnace for one hour at 500 ºC. The residue was then leached in a mixture of 1 M HCl and 4% H_2O_2 at 80 ºC for two hours, cooled, and sieved to produce graphite residue, which was further used as the electrode material in combination with carbon nanotubes.

Preparation of bare composite electrode

Using an agate mortar and pestle, the waste carbon, carbon nanotubes, and silicone oil were mixed in a 50:20:30 ratio to create the paste that was required for the creation of the functioning electrode. To achieve a consistent surface, the prepared paste was thus filled into the hollow area of the Teflon rod (3 mm internal diameter) and its exterior was rubbed over the tissue paper. The prepared Teflon tube served as the electrode for the bare composite. Copper wire was then introduced at the opposite end of the electrode to provide an electrical connection between it and the electrochemical analyzer.

Acknowledgements Dr. J.G. Manjunatha gratefully acknowledges the financial support from VGST, Bangalore under the Research project No. K-FIST (L2)/GRD-1020/2022-23/430. Nagaraja Sreeharsha gratefully acknowledges the financial support from the Deanship of Scientific Research, Vice Presidency for Graduate Studies and Scientific Research, Grant No. KFU252781, King Faisal University, Saudi Arabia.

Data availability Data will be made available on reasonable request.

Declarations

Conflict of interest The authors declare that they have no known competing financial interests or personal relationships that could have appeared to influence the work reported in this paper.

References

1. Itagaki S, Kurokawa T, Nakata C, Saito Y, Iseki K, Hirano T (2009) Food Chem 114:466
2. Shi Y, Chen X, Qiang S, Su J, Li J (2021) Int J Mol Sci 22:11305
3. Pueknang J, Saewan N (2022) Molecules 27:3463
4. Kanski J, Aksenova M, Stoyanova A, Butterfield DA (2002) J Nutr Biochem 13:273
5. Peres DD, Sarruf FD, de Oliveira CA, Velasco MVR, Baby AR (2018) J Photochem Photobiol B: Biol 185:46
6. Choi JH, Park JK, Kim KM, Lee HJ, Kim S (2018) J Biochem Mol Toxicol 32:e22004
7. Pandi A, Chakraborty B, Sen N, Kalappan VM (2025) Arch Toxicol 99:2229
8. Di Giacomo S, Percaccio E, Gullì M, Romano A, Vitalone A, Mazzanti G, Gaetani S, Di Sotto A (2022) Nutrients 14:3709
9. Liu L, Gou Y, Gao X, Zhang P, Chen W, Feng S, Hu F, Li Y (2014) Mater Sci Eng C 42:227
10. de Paiva LB, Goldbeck R, dos Santos WD, Squina FM (2013) Braz J Pharm Sci 49:395
11. Fu L, Chen Q, Chen J, Ren L, Tang L, Shan W (2021) J Chromatogr B 1180:122870
12. Júnior JVC, Muniz VM, de Almeida VCR, de Souza FS, Aragão CFS (2022) J Sep Sci 45:3866
13. Shweta Tripahi ST (2021) Life Sci Leafl 135:21
14. Stoicescu I, Lupu EC, Radu MD, Popescu A, Mihai S (2022) Anal Lett 55:2147
15. Balkrishna A, Joshi M, Gupta S, Rani MP, Srivastava J, Nain P, Varshney A (2024) Heliyon 10:e35918
16. Liu H, Liu Y, Han H, Lu C, Chen H, Chai Y (2023) Food Chem 424:136402
17. Sgarbossa A, Monti S, Lenci F, Bramanti E, Bizzarri R, Barone V (2013) Biochim Biophys Acta 1830:2924
18. Agrawal S, Kalor H, Ghadge K, Patil G, Mohite V, Bunage B, Jadhav A (2025) JPC – Journal of Planar Chromatography – Modern TLC 38:59
19. Yang S, Han Y, Wang K, Wang Y, Li L, Li N, Xu X (2021) RSC Adv 11:33996
20. Ebrahimi P, Shahidi SA, Bijad M (2020) Food Measure 14:3389
21. Bounegru AV, Apetrei C (2020) Sensors 20:6724
22. Beitollahi H, Safaei M, Tajik S (2020) Microchem J 152:104287
23. Halfadji A, Naous M, Rajendrachari S, Ceylan Y, Ceylan KB, Raja Shekar PV (2024) J Mol Struc 1301:137318
24. MohammadzadehJahani P, Zaimbashi R, Aflatoonian MR, Tajik S, Beitollahi H (2024) J Electrochem Sci Eng 14:631
25. Măgeruşan L, Pogăcean F, Soran ML, Pruneanu SM (2023) Int J Mol Sci 24:16937
26. Bounegru AV, Apetrei C (2022) Sensors 22:4689
27. Abdel-Hamid R, Newair EF (2015). Nanomaterials. https://doi.org/10.3390/nano5041704
28. Ebrahimi N, Rafiee-Pour HA, Mahmoodi-Khaledi E (2024) Microchem J 203:110925
29. Elgrishi N, Rountree KJ, McCarthy BD, Rountree ES, Eisenhart TT, Dempsey JL (2018) J Chem Educ 95:197
30. Nurdin M, Agusu L, Putra AAM, Maulidiyah M, Arham Z, Wibowo D, Umar AA (2019) J Phys Chem Solids 131:104
31. Siavashi R, Beitollahi H (2024) Iran J Anal Chem 11:123
32. Deng X, Lin X, Zhou H, Liu J, Tang H (2023) Nanomaterials 13:239
33. BattiraMadappa S, Manjunatha JG, Karnayana M, Mahmoud Osman S, Patra S (2024) J Taibah Univ Sci 18:2359209
34. Karimi-Maleh H, Keyvanfard M, Alizad K, Fouladgar M, Beitollahi H, Mokhtari A, Gholami-Orimi F (2011) Int J Electrochem Sci 6:6141
35. Rajendrachari S, Altaş E, Erdogan A, Küçük Y, Gök MS, Khosravi F (2024) Inorg Chem Comm 167:112426
36. Moallem QA, Beitollahi H (2025) J Environ Bioanal Electrochem 1:1
37. Mahale RS, Rajashekar V, Vasanth S, Chikkegowda SP, Shashanka R, Mahesh V (2024) ACS Omega 9:10660
38. Tajik S, Beitollahi H, Mohammadi SZ, Nejad FG, Dourandish Z (2024) Chem Phys Impact 8:100653
39. Kanthappa B, Manjunatha JG, Osman SM, Ataollahi N (2024) Sci Rep 14:30950
40. Pushpanjali PA, Manjunatha JG, Girish T, Santosh F (2020) Anal Bioanal Electrochem 12:553
41. Hareesha N, Soumya DM, Mounesh, Manjunatha JG, Rohit RN, Manikanta P, Varun DN, Ataollahi N, Thippeswamy BA, Pramoda K, Nagaraja BM (2024) J Environ Chem Eng 12:113584
42. Zahran M, Khalifa Z, Zahran MAH, Azzem MA (2021) Mater Adv 2:7350
43. El Mhammedi MA, Achak M, Hbid M, Bakasse M, Chtaini A (2009) J Hazard Mater 170:590
44. Chang F, Ren K, Li S, Su Q, Peng J, Tan J (2023) Ecotoxicol Environ Saf 252:114588
45. Zhong Y, Liu MM, Chen Y, Yang YJ, Wu LN, Bai F, Lei Y, Gao F, Liu AL (2020) Microchim Acta 187:197
46. Rajendrachari S, Chalageri GR, Mahale RS, Altas E, Chapke Y, Adimule V (2025) Catalysts 15:259
47. Rajendrachari S, Mahale RS, Adimule V, Gulen M, Mahesh V, Basavegowda N (2024) Inorg Chem Comm 164:112428
48. Manjunatha JG, Kanthappa B, Hareesha N, Raril C, Tighezza AM, Albaqami MD (2023) Chem Afr 7:1141
49. Sharmila BM, Manjunatha JG, Amrutha BM, Habila MA, Sillanpaa M (2024) Sens Imaging 25:7
50. Amrutha BM, Manjunatha JG, Hareesha N, Tighezza AM, Albaqami MD, Sillanpaa M (2022) Diagnostics 12:3113
51. Jing L (2017) Int J Electrochem Sci 12:8504
52. Abdel-Hamid R, Newair E (2015) Nanomaterials 5:1704
53. Zhao X, Zhang Y, Gao D, Xiong H, Gao Y, Li S, Li X, Yang Z, Liu M, Dai J, Zhang D (2019) Int J Electrochem Sci 14:506
54. Zabihpour T, Shahidi S, KarimiMaleh H, Ghorbani-HasanSaraei A (2020) Eurasian Chem Commun 2:362
55. Luo L, Wang X, Li Q, Ding Y, Jia J, Deng D (2010) Anal Sci 26:907
56. Zhang Y, Liu Y, Yang Z, Yang Y, Pang P, Gao Y, Hu Q (2013) Anal Methods 5:3834